Antibiotic entrapment in antibacterial micelles as a novel strategy for the delivery of challenging antibiotics from silica nanoparticles

Muguruza, Asier R.; Odyniec, Maria L.; Manhota, Menisha; Habib, Zaina; Rurack, Knut; Blair, Jessica M.A.; Kuehne, Sarah; Walmsley, A. Damien; Pikramenou, Zoe

DOI:
10.1016/j.micromeso.2023.112841

Microporous and Mesoporous Materials 363 (2024) 112841

Contents lists available at ScienceDirect

Microporous and Mesoporous Materials

journal homepage: www.elsevier.com/locate/micromeso

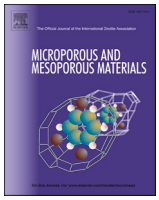

Antibiotic entrapment in antibacterial micelles as a novel strategy for the delivery of challenging antibiotics from silica nanoparticles

Asier R. Muguruza [a,1], Maria L. Odyniec [a,1], Menisha Manhota [a,b], Zaina Habib [a], Knut Rurack [c], Jessica M.A. Blair [d], Sarah A. Kuehne [e], A. Damien Walmsley [e], Zoe Pikramenou [a,*]

[a] School of Chemistry, College of Engineering and Physical Sciences, University of Birmingham, Edgbaston, Birmingham, B15 2TT, United Kingdom
[b] Doctoral Training Centre in Physical Sciences for Health, University of Birmingham, Edgbaston, Birmingham, B15 2TT, United Kingdom
[c] Chemical and Optical Sensing Division, Bundesanstalt für Materialforschung und -prüfung (BAM), Richard-Willstätter-Str. 11, 12489, Berlin, Germany
[d] Institute of Microbiology and Infection, College of Medical and Dental Sciences, University of Birmingham, Edgbaston, Birmingham, B15 2TT, United Kingdom
[e] School of Dentistry, College of Medical and Dental Sciences, University of Birmingham, Birmingham, B5 7EG, United Kingdom

ARTICLE INFO

Keywords:
Cetylpyridinium chloride
Micelles
Nuclear magnetic resonance
Antibiotics
Porous silica nanoparticles
Drug delivery

ABSTRACT

Silica materials are popular in biomedical applications as composites and drug delivery platforms due to their low toxicity and biocompatibility. Mesoporous silica nanoparticles are attractive drug delivery systems based on their porous silica framework with high surface area. In the preparation of mesoporous silica frameworks, most commonly, MCM-41, the efficient removal of the template responsible for introducing porous networks, cetyltrimethyl ammonium bromide (CTAB), is a critical step due to the template's high toxicity in the environment and human health. In this work, we present a new one-pot approach of introducing challenging antibiotics within a silica framework without the need of toxic templates, but instead using micelle formation by an antibacterial agent. We demonstrate that micelles formed by cetylpyridinium chloride (CPC), a known antibacterial agent, entrap antibiotics such as rifampicin and ciprofloxacin. Extensive NMR studies elucidate the precise localisation of the antibiotic within the CPC micelle. Ciprofloxacin is placed between the outer and palisade region while rifampicin is located further into the hydrophobic CPC micelle core. In both cases, the formation of the silica framework can be built around the CPC-antibiotic loaded micelles. The resulting silica nanoparticles show loading of both CPC and antibiotic agents, porosity and dual antibacterial release upon disruption of the micelle within the silica framework. The design not only provides a strategy of a therapeutic design to form porous frameworks but also highlights the potential of precise antibiotic dose and release in nanoparticle systems.

1. Introduction

Designs of efficient delivery systems for antibiotics is a key step in controlling antibiotic dose and ultimately plays a role in combatting antibiotic resistance. Silica nanoparticles (SiO_2) are popular drug delivery systems due to their biocompatibility, facile synthesis and tuneable size, from nanometre to micrometres, shape and surface chemistry for functionalisation. [1] Entrapment of drugs in the silica framework is limited by the drugs' solubility and compatibility with the polarity of the silica network. [2,3] This property is particularly pertinent for hydrophobic antibiotics with challenging inclusion in polar frameworks. One of the common approaches for entrapment of antibiotics is the formation of porous networks within the siliceous framework in order to achieve high surface area for drug loading. [1,4] MCM-41 and SBA-15 are among the most popular mesoporous silica nanoparticle topologies, which are well established for agent inclusion in their porous networks. [1] Their formation is based on surfactant based liquid templates which lead to a periodic mesoporous network after its removal. [5–7] The templates used for porosity formation in MCM-41 and SBA-15 are cetyltrimethylammonium bromide (CTAB) and Pluronic P123, respectively. However, CTAB and Pluronic P123 are highly toxic to aquatic life and potential carcinogens (IC_{50} = 30 μM for CTAB and 12–30 μM for P123) [8,9] and complete removal can be challenging. Additionally, the drug uptake of the mesoporous particles relies on the adsorption of the drug within the pores of the particle which results in uncontrolled dose loading and "burst" release upon dispersion of the particles in a liquid

* Corresponding author.
E-mail address: z.pikramenou@bham.ac.uk (Z. Pikramenou).
[1] These authors contributed equally to this work.

https://doi.org/10.1016/j.micromeso.2023.112841
Received 28 June 2023; Received in revised form 20 September 2023; Accepted 1 October 2023
Available online 5 October 2023

medium. Blocking the pores of the particle with chemical functionalisation has been introduced to control of the drug release which requires additional synthesis steps and a reactive stimulus to enable full control over release. [10,11].

An alternative approach to introducing porosity in silica particles uses antibacterial amphiphiles such as octenidine dihydrochloride, [12] cetylpyridinium chloride (CPC), [13,14] and benzalkonium chloride [15] which all adopted MCM-41 topology. We have been interested in alternative methods for inclusion of agents of interest within the silica framework, accompanied by surface modification for imaging [16–18] and drug delivery. [19].

In this work, we introduce a strategy to deliver challenging antibiotics from silica nanoparticles through entrapping into micelles. We employed CPC, an antibacterial amphiphile with a positively charged quaternary ammonium headgroup and a hexadecyl aliphatic tail, widely used in dental products such as mouthwashes [20] which forms micelles. We have examined the inclusion of rifampicin (RIF) and ciprofloxacin (CPX), as examples of poorly water-soluble antibiotics. RIF has previously been shown to only be included in mesoporous silica by its adsorption in the pores, [21] but direct inclusion within silica framework remains a challenge due to its hydrophobicity. Similarly, CPX loading in silica particles is limited to those mesoporous particles with surface functionalisation to assist adsorption. [22,23] Herein we study the entrapment of the antibiotic in micelles and growth of silica nanoparticles in a one-pot approach in order to incorporate antibiotic within the silica framework and examine their release (Fig. 1).

2. Materials and methods

2.1. Materials

Rifampicin (RIF), cetylpyridinium chloride (CPC) and tetraethoxysilane (TEOS) were purchased from Merck and ciprofloxacin (CPX) was purchased from Fluorophen. Rest of chemicals and consumables were purchased from Merck and were of the highest quality available.

2.2. Synthesis of SiO_2

Synthesis of SiO_2 – general procedure 1. The Stöber method with modifications was used to synthesise the non-porous silica nanoparticles. [24] First a solution containing EtOH (25 mL), NH_4OH (1.9 mL, 0.93 M), H_2O (1.6 mL, 2.9 M) and TEOS (2.4 mL, 12.4 mmol, 1 equiv, 0.41 M) were added together. The reaction was left to stir (750 rpm) for 3 h at rt. After 3 h, a solution of antimicrobials was added and stirred at RT for 6 h. The silica nanoparticles were isolated by centrifugation (15 min, 7830 rpm) and washed with H_2O (3 x 20 mL). After three cycles of the centrifugation-washing procedures, the silica nanoparticles were dried *in-vacuo* to yield a powder.

SiO_2 ⊃ CPC. Following general procedure 1, after 3 h a solution of CPC (0.465 g, 1.36 mmol, 0.1 equiv) in H_2O (3 mL) was added. Nanoparticles were isolated as a white powder (0.54 g).

SiO_2 ⊃ CPX. Following general procedure 1, after 3 h a solution of CPX (0.016 g, 0.048 mmol, 0.004 equiv) in H_2O (3 mL) was added. Nanoparticles were isolated as a white powder (0.17 g).

SiO_2 ⊃ RIF. Following general procedure 1, after 3 h a solution of RIF (0.040 g, 0.048 mmol, 0.004 equiv) in EtOH (3 mL) was added. Nanoparticles were isolated as a white powder (0.28 g).

SiO_2 ⊃ CPC-CPX. Following general procedure 1, after 3 h a premixed solution of CPX (0.016 g, 0.048 mmol, 0.004 equiv) and CPC (0.465 g, 1.36 mmol, 0.1 equiv) in H_2O (3 mL) was added. Nanoparticles were isolated as a white powder (0.19 g).

SiO_2 ⊃ CPC-RIF. Following general procedure 1, after 3 h a premixed solution of RIF (0.040 g, 0.048 mmol, 0.004 equiv) and CPC (0.465 g, 1.36 mmol, 0.1 equiv) in EtOH/H_2O (1/3 mL) was added. Nanoparticles were isolated as an orange powder (0.41 g).

2.3. Quantification of antibiotics loaded by UV/Vis

UV/Vis absorption measurements were carried out to determine the amount of antibiotics loaded into the materials using the lowest-energy absorption maximum (Abs_{max}). The concentration of each antibiotic in synthesis conditions were measured before adding to synthesis mixture. Then after synthesis, all supernatants and washings were collected to measure the remaining antibiotic in solution by absorption and analysis via the *Beer-Lambert* law.

Encapsulation efficiency (*EE* in %) is calculated as the percentage of drug that is successfully entrapped into the nanoparticle eq (1):

$$EE = \left(\frac{total\ drug\ added - free\ non\ entrapped\ drug}{total\ drug\ added}\right) \text{x } 100 \qquad \text{eq (1)}$$

The encapsulation efficiency is converted into weight percent (wt%) eq (2):

$$wt = \frac{(EE)\ x\ total\ drug\ added}{mass\ of\ nanoparticles\ synthesised} \qquad \text{eq (2)}$$

2.4. Release studies

Release studies were performed using loaded SiO_2 suspensions (2 mg/mL) in water or in methanol at 25 °C under stirring (750 rpm) for up to 48 h. Aliquots (0.5 mL) were taken at set time points, then centrifuged (5 min at 14000 rpm) to remove nanoparticles and released CPC, CPX and RIF quantified by measuring the remaining supernatant, using a Cary 60 UV/Vis spectrometer by absorption and analysis via the *Beer-Lambert* law. The release experiments were repeated three times.

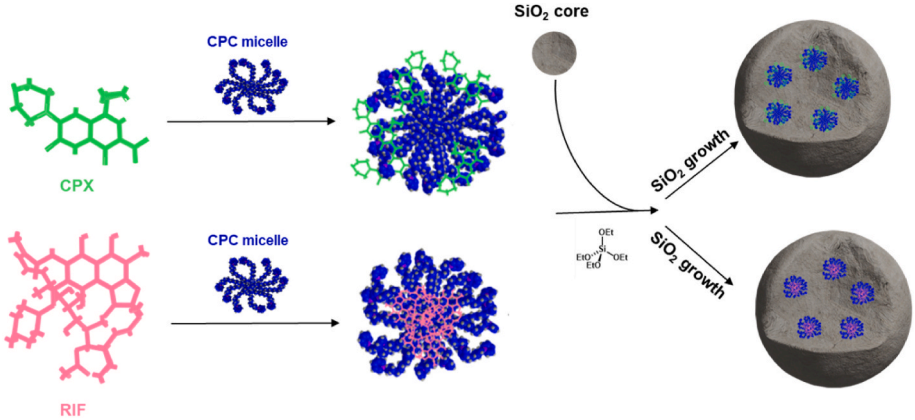

Fig. 1. Scheme of the antibiotic entrapment in CPC micelles and their inclusion in SiO_2 nanoparticles.

3. Results and discussion

3.1. Characterisation of CPC micelle-antibiotic interactions

CPC micelle formation has been previously investigated and the critical micelle concentration (CMC) is widely agreed to be 1 x 10^{-3} M in pH neutral aqueous systems at 25 °C. [25–27] In addition, computational DFT simulations have been able to elucidate the most energetically favourable conformation in different solvents, showing that the aliphatic chains are non-linear. [27] In this study, we first investigated the **CPC** micelles by Dynamic Light Scattering (DLS). We used a **CPC** concentration of 2 mM which is above the CMC and carbonate buffer (0.1 M, pH 10.6) as dispersing medium to mimic the SiO_2 nanoparticles synthesis conditions (pH 10.5). [28] Under these conditions, CPC micelles are formed with a hydrodynamic diameter of 4.9 ± 1.2 nm (Fig. S1, Table S1).

Titrations of antibiotics, **CPX** or **RIF**, into a solution of **CPC** micelles (2 mM) shows an increase in hydrodynamic diameter with increase in antibiotic concentration up to 6 mM (Fig. 2): from 4.9 ± 1.2 nm to 6.8 ± 1.2 nm for addition of **CPX** and 7.5 ± 1.2 nm for addition of **RIF**. An increase in micelle size is previously reported, for other drugs incorporated or associated within micelles. [29–31] The ζ-potentials of unloaded **CPC** micelles display a positive value of +23 ± 2 mV, due to positively charged pyridinium heads on micelle-water interface. [27] The ζ-potential decreases to +15 ± 1 mV and +19 ± 1 mV upon addition of **CPX** or **RIF**, respectively. This decrease is attributed to changes in electron density at the pyridinium head of **CPC** at pH 10.6. [32,33].

In order to further evidence the interactions between **CPC** micelles and antibiotics we used Nuclear Magnetic Resonance (NMR) techniques. **CPC** micelle formation is confirmed by ^{1}H NMR. As the concentration of **CPC** increases from 0.5 mM (<CMC) to 2 mM (>CMC), characteristic shifts in proton resonances are observed (Fig. S2, Table S2). The pyridinium protons $H_{1,5}$ (δ = 8.89 ppm) and alkyl protons H_7 (δ = 1.94 ppm) and H_8 (δ = 4.63 ppm) show upfield shifts ($\Delta\delta$ = +0.01–0.03 ppm), while the remaining proton resonances of the aliphatic tail H_{9-22} (δ = 1.08–1.26 ppm) show downfield shifts. These data indicate a change in the environment of **CPC** upon micelle formation and is supported by previous studies undertaken in D_2O. [34,35] Above the CMC (45 mM), **CPC** micelles show intermolecular interactions in the NOESY which are not present in the COSY (Fig. S3). The CPC micelles show additional interactions between pyridinium protons $H_{2,4}$ (δ = 8.08 ppm) and $H_{1,5}$ (δ = 8.89 ppm) with aliphatic protons H_{9-21} (δ = 1.08–1.26 ppm). There are also intermolecular interactions between H_8 (δ = 4.63 ppm) with H_{9-21} (δ = 1.08–1.26 ppm) and H_8 (δ = 4.63 ppm) with pyridinium protons $H_{1,5}$ (δ = 8.89 ppm), supporting close proximity of **CPC** molecules.

Firstly, we investigated the proton shifts upon addition of **CPX** (^{1}H NMR before addition, Fig. S4) to **CPC** micelles (1:12). **CPX** is a poorly water-soluble molecule. [36,37] The pKa values for **CPX** are 5.90 and 8.89 and are associated to the carboxylic acid group and the amine in the piperazine group, respectively. [38] At pD 10.6, it is likely that the carboxylate will interact with the positively charged pyridinium group. In the presence of **CPX**, the ^{1}H NMR spectra of **CPC** micelles show small upfield shifts except for the terminal methyl protons (H_{22}, δ = 0.77 ppm) which show no shifts (Fig. S5, Table S3). This phenomenon indicates that the presence of **CPX** changes the molecular environment of **CPC** protons. The upfield trend in ^{1}H proton resonance shifts has been reported as evidence between cationic micelles and aromatic molecules. [35,39] As the terminal methyl groups in **CPC** micelles were not affected by **CPX**, this suggests the location of **CPX** is at the micelle-water interface, as previously described for polar molecules on addition to both anionic and cationic surfactant micelles. [35,39,40] Additionally, there are changes in the ^{1}H NMR resonances of **CPX** in the presence of **CPC** micelles. Similar to **CPC** micelles the **CPX** proton resonances show upfield shifts except for the cyclopropane proton H^x_{11}. However, the fine structures of the splitting patterns change with those of the piperazine protons $H^x_{20,24}$ and cyclopropane protons H^x_{11} and $H^x_{19,18}$ appear broadened and the aromatic protons H^x_6, H^x_3, H^x_8 appear with two sets of resonances. These patterns may indicate the molecules are in different environments affected either by the viscosity of solution, [39] local environments [41] or changes in molecular tumbling. [42] The significant changes observed in ^{1}H NMR spectra of **CPX** in the aromatic region may be attributed to interactions of the negatively charged π system of **CPX** with the positively charged pyridinium group of **CPC** through cation-π interactions. [43–45].

The interactions between **CPC** micelles and **CPX** are further investigated by NOESY studies. Two significant NOEs are observed between **CPC** and **CPX** (Fig. 3). One NOE corresponds to the interaction between the protons of the cyclopropane ring (H^x_{18}, H^x_{19}) at δ = 0.85 ppm of **CPX** and the aliphatic chain protons of **CPC** (H_{9-21}) at δ = 1.30 ppm. The other NOE corresponds to the H^x_{11} proton on the cyclopropane ring at δ = 3.5 ppm and the aliphatic chain protons of **CPC** (H_{9-21}) at δ = 1.30 ppm. The NOEs for **CPC** micelle interactions do not change in the presence of **CPX** which indicates that the micelle has not broken apart, this is also supported by DLS studies. For the **CPC** micelles a new NOE is observed between **CPC** pyridinium protons $H_{1,5}$ (δ = 8.89 ppm) and neighbouring **CPC** protons H_7 (δ = 1.94 ppm), suggesting a closer interaction of these protons within the **CPC** micelles through-space than without **CPX**. The shifts in ^{1}H NMR spectra and presence of NOEs indicate that the cyclopropane ring of **CPX** is interacting with the aliphatic tails of **CPC** micelles in the palisade layer of the micelle, namely between the hydrophilic groups and first few carbon atoms of hydrophobic groups [45] as there is no change in resonance of the terminal protons of H_{22} (δ = 0.77 ppm). In addition, cation-π interactions between pyridinium headgroups of **CPC** micelles and **CPX** aromatic protons (H^x_6, H^x_8, H^x_3) at δ = 7.74 ppm, δ = 7.53 ppm and δ = 8.49 ppm, illustrate the **CPX** molecule is sitting at the micelle-water interface, with the piperazine group ($H^x_{20\text{-}24}$ at δ = 3.24–2.28 ppm) pointing outwards as there is an absence of NOEs and the piperazine group is able to hydrogen bond with solvent molecules.

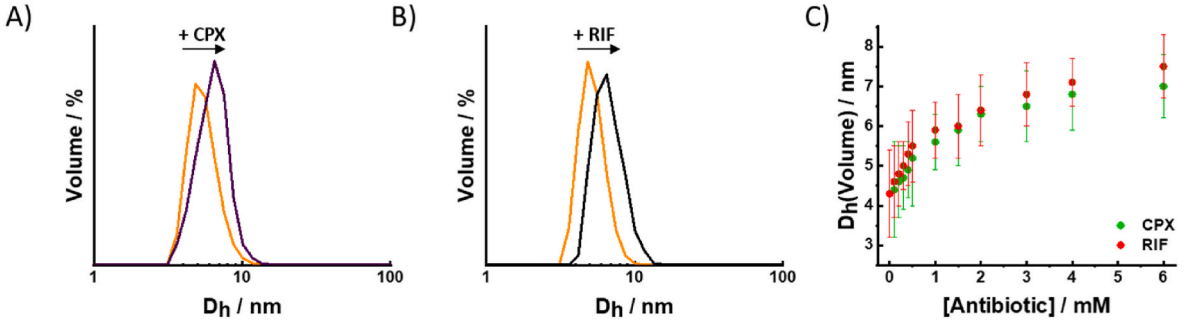

Fig. 2. Dynamic light scattering for monitor the hydrodynamic diameter (volume distribution) of CPC micelles (2 mM) upon addition of antibiotics (A) **CPX** and (B) **RIF** in carbonate buffer (HCO_3^-/CO_3^{2-}, 0.1 M, pH 10.6).

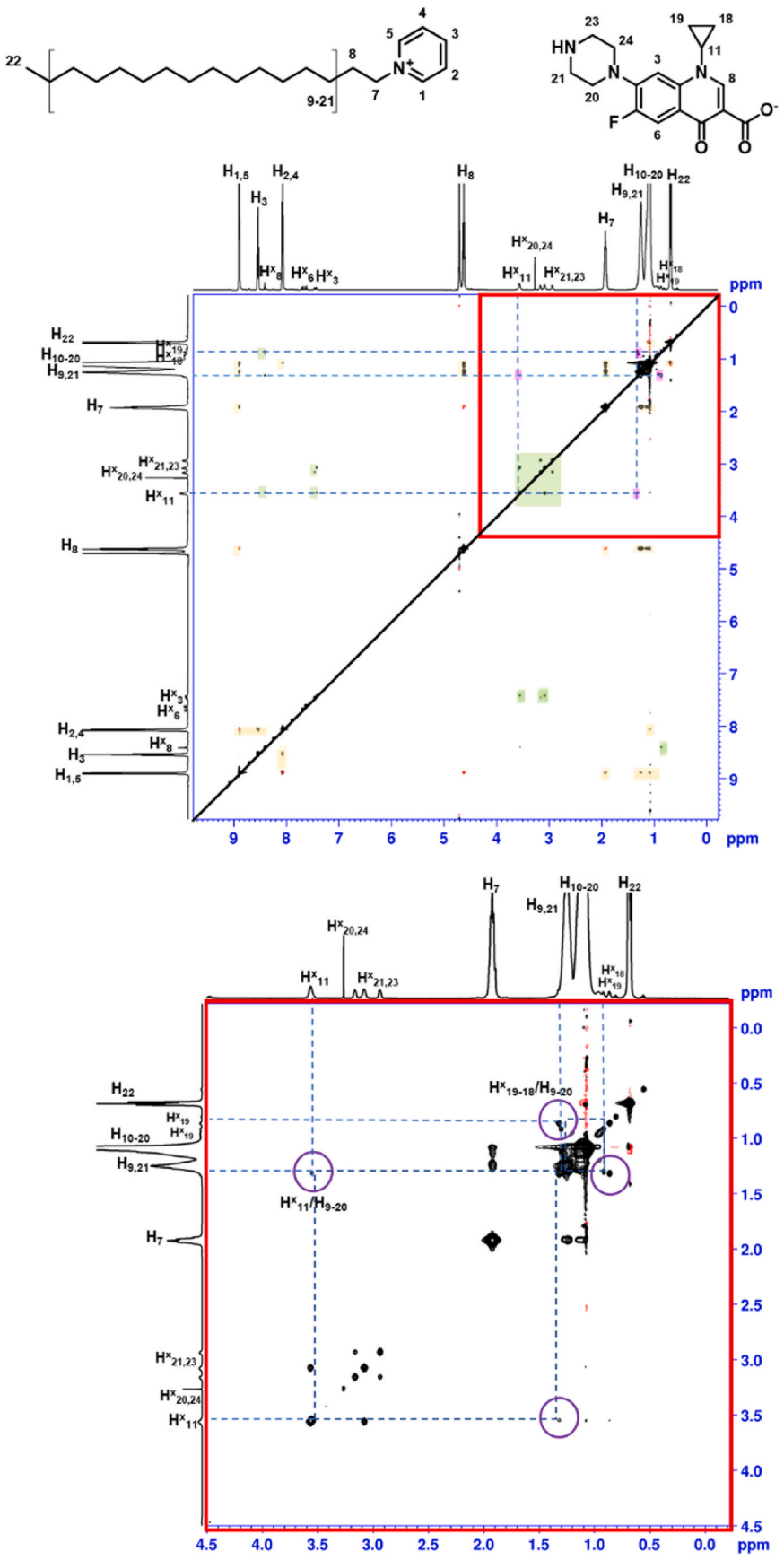

Fig. 3. 500 MHz NOESY spectra of **CPX** and **CPC** (1:12) in carbonate buffer (HCO_3^-/CO_3^{2-}, 0.1 M, pH 10.6). **CPX** cross peaks are labelled in green, **CPC** cross peaks are labelled in yellow. **CPC-CPX** cross peaks are labelled as purple boxes.

We also studied the proton shifts to determine interactions between **RIF** and **CPC** micelles. In the presence of **RIF**, the ^{1}H NMR spectra of **CPC** micelle show shifts in proton resonances. The proton resonances show small upfield shifts except for the terminal methyl protons of **CPC**, H_{22} ($\delta = 0.81$ ppm) and bulk aliphatic protons H_{10-20} ($\delta = 1.20$ ppm) which show downfield shifts (Fig. S6, Table S4); indicating that **RIF** is situated further into the core of the micelle. The pKa values of **RIF** are 1.7 and 7.9, relating to the 4-hydroxy and 3-piperazine nitrogen respectively. Thereby, under basic conditions (pD = 10.6), **RIF** is neutral and converted to **RIF** quinone. [46] The ^{1}H NMR spectrum of **RIF** in carbonate buffer shows the presence of two species; one major and one minor, indicated by additional peaks in the spectra (Fig. S7). It is reported in mildly basic conditions **RIF** can slowly undergo deacetylation to form 22-desacetylrifampin and hydrolysis to formyl-rifampicin can also occur. [46] In the presence of **CPC**, the ^{1}H NMR shows a single set of **RIF** resonances, the fine structure of the resonance peaks of **RIF** merge together changing from sharp and narrow to smooth and wide in the presence of **CPC** micelles. The protons of **RIF** show upfield shifts ($\Delta\delta$ = 0.03–0.15 ppm) except for the resonance of H^R_{25} and H^R_{31} which have small ($\Delta\delta$<0.05 ppm) downfield shifts.

There are a significant number of NOEs between **RIF** and **CPC** (Fig. 4). In general, most of the NOEs are between the aliphatic chain of **CPC** and **RIF** than with the pyridinium head of **CPC**. NOEs are observed between **RIF** piperazine protons H^R_{54-57} ($\delta = 3.05$ ppm, $\delta = 2.49$ ppm), **RIF** piperazine *N*-methyl H^R_{58} ($\delta = 2.22$ ppm) and **CPC** pyridinium head protons $H_{2,4}$ ($\delta = 8.14$ ppm). The **RIF** methyl group H^R_{31} ($\delta = 0.61$ ppm) also shows a cross peak with proton $H_{2,4}$ ($\delta = 8.14$ ppm) of **CPC**. An additional cross peak between the pyridinium head of **CPC** and **RIF** is observed between **CPC** $H_{1,5}$ ($\delta = 8.93$ ppm) and **RIF** *O*-methoxy protons H_{59} ($\delta = 2.96$ ppm). **RIF** alkene protons H^R_4 ($\delta = 6.51$ ppm), H^R_5 ($\delta = 6.29$ ppm), H^R_{35} ($\delta = 6.13$ ppm), H^R_1 ($\delta = 5.99$ ppm), H^R_{25} ($\delta = 5.16$ ppm), show NOEs exclusively with **CPC**'s aliphatic protons H_{22} ($\delta = 0.82$ ppm), H_{9-21} ($\delta = 1.27$ ppm) and H_8 ($\delta = 1.97$ ppm). However, the **RIF** alkene proton H^R_{22} ($\delta = 5.02$ ppm) shows NOEs only with **CPC** H_{9-21} ($\delta = 1.27$ ppm) and H_8 ($\delta = 1.97$ ppm), which illustrates that alkene H^R_{22} ($\delta = 5.02$ ppm) is oriented away from terminal **CPC** micelle protons H_{22} ($\delta = 0.82$ ppm).

The NOEs for **CPC** micelle interactions do not change in the presence of **RIF** which indicates that the micelle has not broken apart and this is also supported by DLS studies. Multiple additional NOEs are observed for **CPC** micelles only. There is a new NOE interaction within the **CPC** micelles between H_7 ($\delta = 1.94$ ppm) and pyridinium protons $H_{1,5}$ ($\delta = 8.89$ ppm) as well as new **CPC** micelle NOEs of H_7 ($\delta = 1.94$ ppm) with pyridinium protons $H_{2,4}$ ($\delta = 8.08$ ppm), aliphatic protons H_{9-21} ($\delta = 1.08–1.26$ ppm) and terminal alkyl protons H_{22} ($\delta = 0.68$ ppm). In addition, aliphatic proton H_8 ($\delta = 4.63$ ppm) has two additional NOEs with pyridinium protons $H_{2,4}$ ($\delta = 8.08$ ppm) and H_3 ($\delta = 8.55$ ppm). H_3 ($\delta = 8.55$ ppm) has an extra interaction with alkyl protons H_{9-21} ($\delta = 1.08–1.26$ ppm). Finally, terminal alkyl protons H_{22} ($\delta = 0.68$ ppm) have two additional NOEs with pyridinium protons $H_{2,4}$ ($\delta = 8.08$ ppm) and $H_{1,5}$ ($\delta = 8.89$ ppm).

Overall, the significant number of NOEs described between the aliphatic chain of **CPC** micelles and **RIF** indicate the presence of **RIF** on the inside of the **CPC** micelle within the hydrophobic core. Specifically, the NOEs between **CPC** terminal alkyl protons (H_{22}) and rifampicin protons, H^R_4, H^R_5, H^R_{35}, H^R_1, and H^R_{25}. This is supported by an increased number of NOEs for the **CPC** micelle itself, which indicates a new arrangement of aliphatic tails inside the micelle in the presence of **RIF**. NOEs between the piperazine protons H^R_{54-57} at $\delta = 3.05$ ppm and $\delta = 2.49$ ppm and piperazine *N*-methyl H^R_{58} at $\delta = 2.22$ ppm of **RIF** and pyridinium protons of **CPC** at $H_{2,4}$ ($\delta = 8.14$ ppm) support orientation of piperazine group of **RIF** towards the pyridinium headgroup of **CPC** micelles within the palisade layer. In addition, the single set of proton resonances observed in ^{1}H NMR for **RIF** in the presence of **CPC** indicates that this interaction may protect **RIF** from hydrolysis and degradation, which is important for maintaining bioavailability of **RIF**. [46,47].

The interaction of the **CPX** and **RIF** with **CPC** micelles were further explored by Isothermal Titration Calorimetry (ITC). Upon titration of the antibiotics into a 2 mM **CPC** micellar solution in carbonate buffer, K_D value of 6.30 ± 0.7 μM for **CPX** and 1.96 ± 0.05 μM for **RIF** with **CPC** micelles (Fig. 5) were calculated.

Additionally, optical spectroscopy was employed to further explore the interactions between the antibiotics and **CPC**. The absorption properties of **CPX** and **RIF** were investigated in a **CPC** micellar medium at pH 10.6. The UV–Vis spectra of **CPC** show a single absorption band with maximum at 259 nm ($\varepsilon = 4190\ M^{-1}cm^{-1}$) (Fig. S8). In carbonate buffer **CPX** has two absorption bands at 270 nm ($\varepsilon = 39000\ M^{-1}cm^{-1}$) and 325 nm ($\varepsilon = 17000\ M^{-1}cm^{-1}$). Due to the overlapping between the higher energy absorption band of **CPX** with **CPC**, changes in this band cannot be monitored. However, at 325 nm, in the presence of **CPC** (6 mM, >CMC), there is a bathochromic shift to 334 nm ($\Delta\lambda = +9$ nm) (Fig. 6A). Similarly, **RIF** has two absorption bands at 334 nm ($\varepsilon = 13000\ M^{-1}cm^{-1}$) and 479 nm ($\varepsilon = 8000\ M^{-1}cm^{-1}$) corresponding to $\pi \rightarrow \pi^*$ transitions. In the presence of **CPC** (6 mM, >CMC), there is a bathochromic shift in both absorption bands of **RIF** to 339 nm ($\Delta\lambda = +5$ nm) and 490 nm ($\Delta\lambda = +11$ nm) with a change in shape of the lower energy absorption band (Fig. 6B). These data indicate that in the presence of **CPC** micelles there is a change in environment for the antibiotics, supporting the interactions described by NOESY.

Furthermore, the change of the environment upon micelle formation was also investigated by steady-state and time resolved fluorescence spectroscopy (Fig. 6C and D). **CPX** displays a maximum emission wavelength at 425 nm upon excitation at 340 nm at pH 10.6. However, after addition of **CPC** (2 mM), **CPX** emission suffers a significant decrease in intensity of 93%. Accordingly, time-revolved fluorescence studies showed a decrease in luminescence lifetime decay ($\lambda_{exc} = 375$ nm, $\lambda_{em} = 425$ nm) upon **CPC** addition from 7.3 ns to 3.3 ns. The spectroscopic observations indicate that there is a change of the environment of **CPX** which quenches the luminescence. There may be aggregation-induced quenching which has been previously described for other fluoroquinolines, [48,49] caused by the close proximity of **CPX** molecules within the **CPC** micelle, or quenching from **CPC** as observed for other anionic aromatic fluorescent dyes. [49].

3.2. Development of silica nanoparticles with CPC micelle loaded antibiotics

Taking advantage of the **CPC-antibiotic** interactions, we used the micelle incorporation to form SiO_2 nanoparticles for delivery of dual antimicrobials. Briefly, a silica core is firstly formed for 3 h, then a solution containing CPC micelles with or without antibiotic of choice is added and silica growth continued for 6 h (Fig. S9). The size of micelles in the synthesis was studied by Transmission Electron Microscopy (TEM) (Fig. 7). TEM of **CPC-CPX** micelles reveals two populations with average sizes of 3 ± 2 nm (n = 50) and 7 ± 2 nm (n = 50), while **CPC-RIF** micelles show a single population of 5 ± 1 nm (n = 50) (Fig. S15). The two populations of **CPC-CPX** micelles in TEM can be attributed to the drying process before imaging. Subsequently, the sizes of synthesised silica nanoparticles were explored by Scanning Electron Microscopy (SEM). The average nanoparticle sizes are 230 ± 25 nm for **SiO_2 ⊃ CPC-CPX** and 300 ± 20 nm for **SiO_2 ⊃ CPC-RIF** (n = 50). Confirmation of the presence of antibiotics was obtained by solid-state absorption spectroscopy (Fig. 7) of powders of the silica particles, **SiO_2 ⊃ CPC-CPX** and **SiO_2 ⊃ CPC-RIF** which show absorption bands at 340 nm and 330 nm and 480 nm, respectively, characteristic of the presence of **CPX** and **RIF** antibiotics.

Loading of incorporated antibiotics in nanoparticles was calculated by UV/Vis spectroscopy based on remaining antibiotic in the synthesis media and washings. An encapsulation efficiency of 84%, corresponding to 7.2 wt% (72 $\mu g_{CPX}/mg_{NP}$) of **CPX SiO_2 ⊃ CPC-CPX** was calculated. In the absence of CPC, the encapsulation efficiency of **CPX** decreases to 35%, corresponding to 3.0 wt% (30 $\mu g_{CPX}/mg_{NP}$). An encapsulation

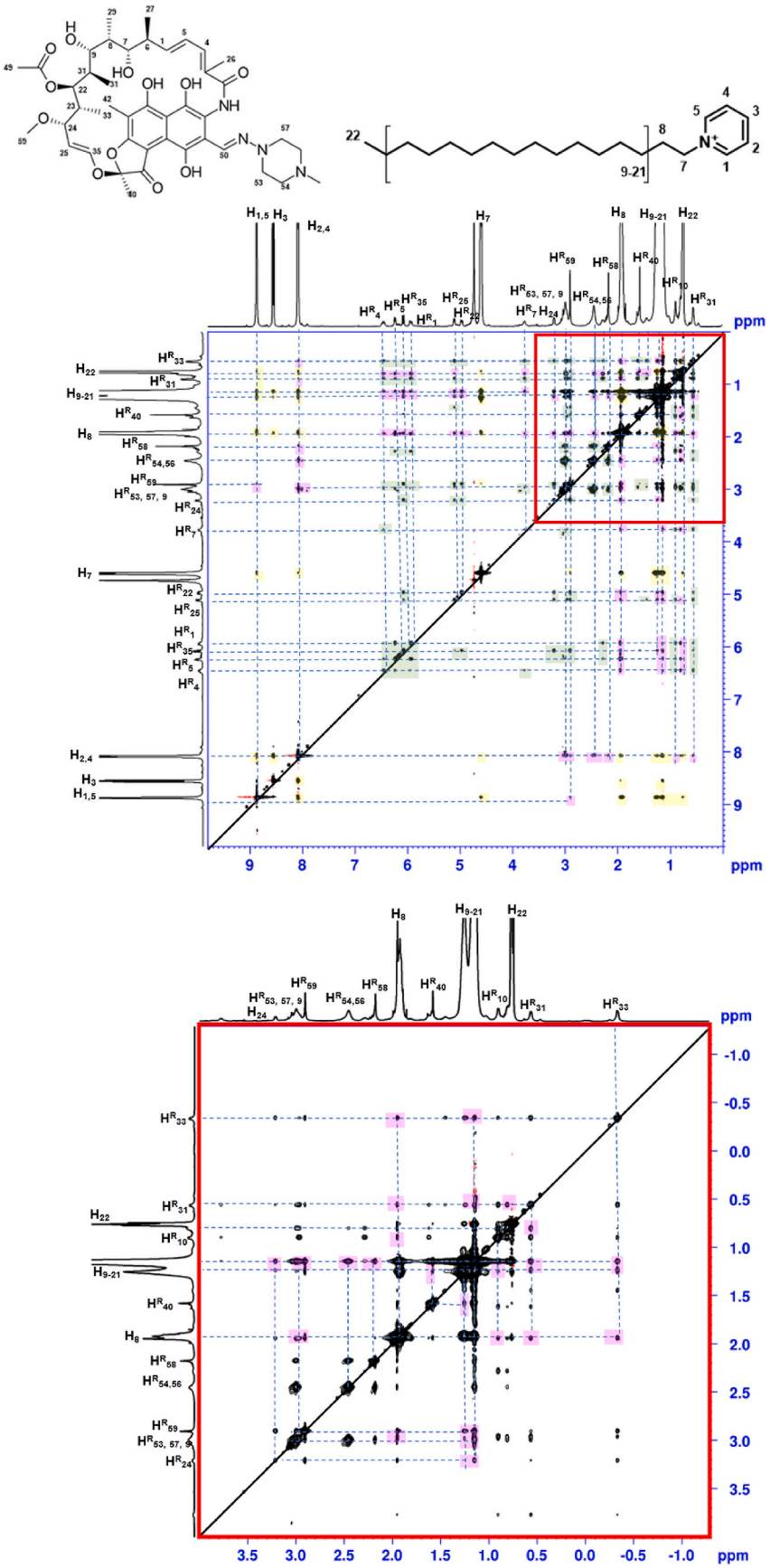

Fig. 4. 500 MHz NOESY 1H NMR spectra of **RIF** and **CPC** (1:12) in carbonate buffer (HCO_3^-/CO_3^{2-}, 0.1 M, pH 10.6). **RIF** cross peaks are labelled in green; **CPC** cross peaks are labelled in yellow. **CPC-RIF** cross peaks are labelled as purple boxes.

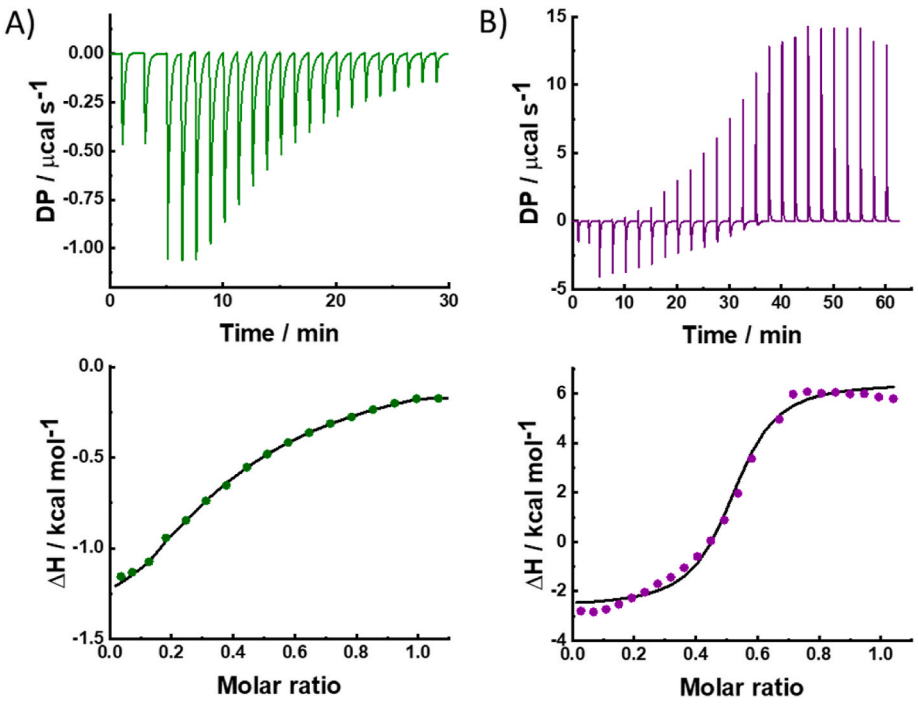

Fig. 5. Isothermal Titration Calorimetry (ITC) profiles showing antibiotic interaction with **CPC** micelles. (A) **CPX** and (B) **RIF** titration on **CPC** (2 mM) in carbonate buffer (HCO_3^-/CO_3^{2-}, 0.1 M, pH 10.6).

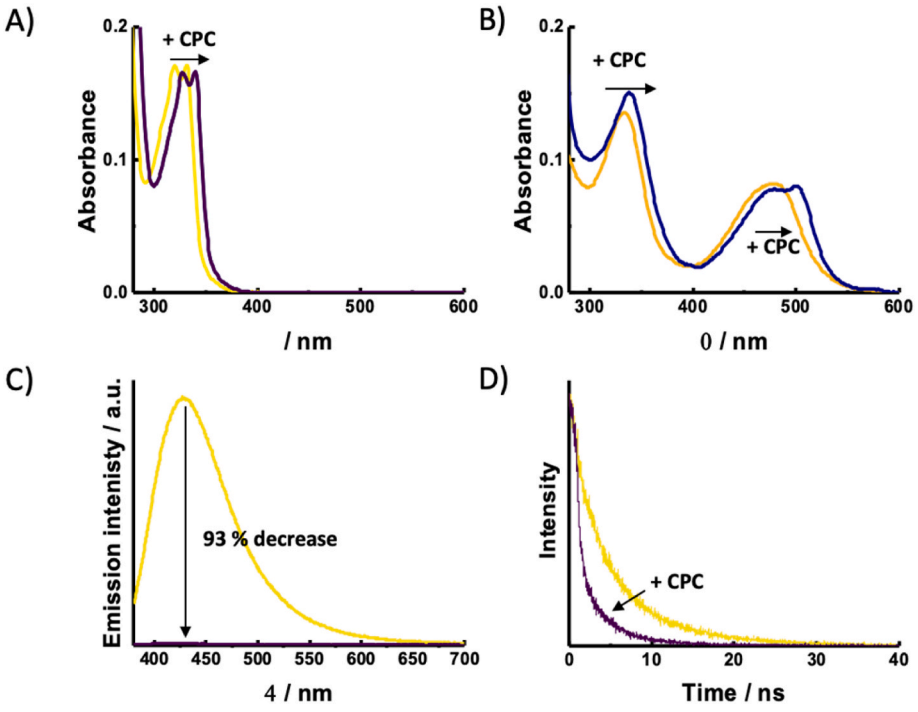

Fig. 6. Optical spectroscopy of antibiotics in presence of **CPC**. UV/Vis absorption spectra of (A) **CPX** (10 µM) and (B) **RIF** (10 µM) upon addition of **CPC** up to 6 mM in carbonate buffer (HCO_3^-/CO_3^{2-}, 0.1 M, pH 10.6), **CPC** absorption band is omitted for clarity. (C) Steady state (λ_{exc} = 340 nm) and (D) time-resolved exponential fluorescence decay (λ_{exc} = 375 nm, λ_{em} = 425 nm) of a **CPX** solution (10 µM) before and after addition of **CPC** (2 mM) in carbonate buffer (HCO_3^-/CO_3^{2-}, 0.1 M, pH 10.6).

efficiency of 20%, corresponding to 2.5 wt% (25 $\mu g_{RIF}/mg_{NP}$) for **RIF** in **SiO_2 ⊃ CPC-RIF** was determined, whereas no loading was achieved in absence of **CPC**. Loading of **CPC**, however, is similar in all nanoparticles, calculated to be between 8% (125 $\mu g_{CPC}/mg_{NP}$) and 11% (195 $\mu g_{CPC}/mg_{NP}$). Thermogravimetric analysis (TGA) is used for the determination of loading of drugs in silica nanoparticles based on continuous monitoring of sample weight loss upon heating at a defined rate under a controlled atmosphere. The amount of organic composition (µg/mg) was calculated from the TGA weight loss from 150 to 900 °C. TGA analysis of CPC shows a single weight loss step at 180–250 °C and 100%

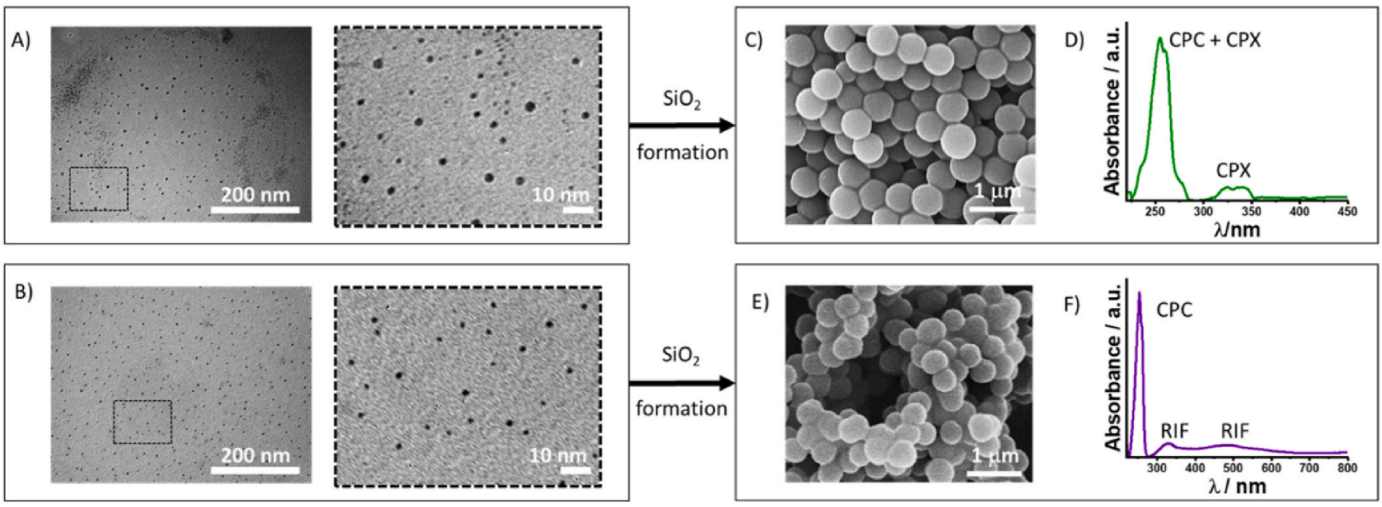

Fig. 7. Characterisation of CPC-antibiotic micelles and corresponding silica nanoparticles. TEM images of (A) **CPC-CPX** and (B) **CPC-RIF** micelles in carbonate buffer (HCO_3^-/CO_3^{2-}, 0.1 M, pH 10.6) to mimic conditions in synthesis. SEM images of (C) **SiO_2⊃CPC-CPX** and (E) **SiO_2⊃CPC-RIF** Solid state absorption spectra of (D) **SiO_2⊃CPC-CPX** and (F) **SiO_2⊃CPC-RIF**.

degradation. TGA analysis of **SiO_2⊃CPC** shows a weight loss of 9.8% compared to unloaded **SiO_2**, corresponding to encapsulation of CPC and loading of 98 $\mu g_{CPC}/mg_{SiO2}$. In comparison the **SiO_2⊃CPC-CPX** and **SiO_2⊃CPC-RIF** particles showed a loss of weight of 18.0% and 18.5% weight loss compared to unloaded **SiO_2**, corresponding to total organic content. These data are consistent with calculation of loading by UV/Vis spectroscopy where total organic content is calculated as 15.2% and 13.5% for **SiO_2⊃CPC-CPX** and **SiO_2⊃CPC-RIF** particles respectively.

Nitrogen adsorption-desorption isotherm studies at 77 K were employed to study the porous structure of nanoparticles (Fig. 8). Nanoparticles were subjected to a calcination process in order to fully remove the antibiotic template. After calcination, it was calculated a BET surface area of 153 ± 3 m^2g^{-1} for **SiO_2 ⊃ CPC**. Similarly, analysis of **SiO_2 ⊃ CPC-CPX** and **SiO_2 ⊃ CPC-RIF** after calcination, resulted in a calculated BET surface area of 215 ± 4 m^2g^{-1} and 334 ± 5 m^2g^{-1}, respectively. Before calcination, and due to the presence of CPC-antibiotic micelles within the porous structure, BET surface areas of 17 ± 1 m^2g^{-1}, 5 ± 1 m^2g^{-1} and 5 ± 1 m^2g^{-1} were calculated for **SiO_2 ⊃ CPC**, **SiO_2 ⊃ CPC-CPX** and **SiO_2 ⊃ CPC-RIF**. Before calcination, N_2 adsorption-desorption isotherm of nanoparticles exhibit a Type I(a) isotherm, according to IUPAC classification, characteristic of microporous materials with relatively low surface area. The increase on adsorbed gas at high P/P_0 is associated with intraparticle spaces. After calcination process, nanoparticles display a Type II isotherm characteristic of microporous material with wider pore size range from micropores (<1 nm) to narrow mesopores (≤2.5 nm). The absence of type IV isotherm and type H1 hysteresis loop suggests the absence of unidimensional pores within nanoparticles.

Recorded isotherms, proves the ability of **CPC** to act as template during the silica formation. Furthermore, calculated average pore size for **SiO_2 ⊃ CPC** was 2.5 nm, which is in good agreement with micelle size simulations [27] and proves the ability of the **CPC** micelles to form a porous structure within the silica framework. In case of **SiO_2 ⊃ CPC-CPX** and **SiO_2 ⊃ CPC-RIF** average pore size of 2.7 nm and 2.8 nm were estimated, respectively with a cumulative pore volume of 1.37 cm^3/g and 1.33 cm^3/g. However, estimated pore sizes may not be reflected accurately given the changes in silica structure upon calcination (Fig. 8). [50] These data illustrate that the presence of the antibiotic does not

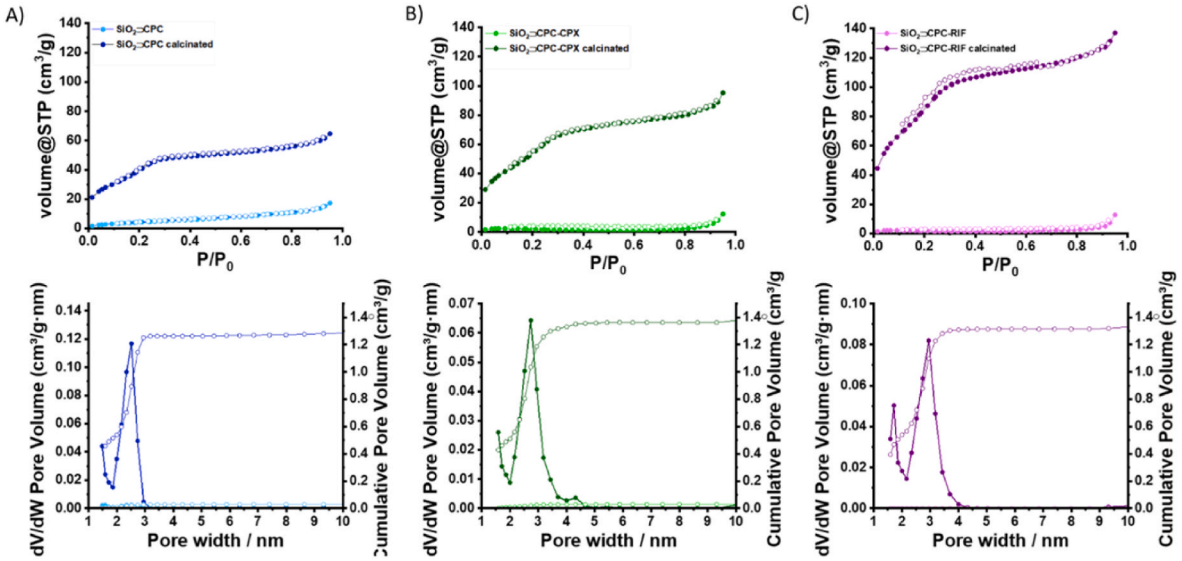

Fig. 8. Nitrogen adsorption-desorption isotherm at 77 K and calculated pore size distribution of (A) **SiO_2⊃CPC,** (B) **SiO_2⊃CPC-CPX** and (C) **SiO_2⊃CPC-RIF** as synthetized and after calcination treatment at 600 °C for 18 h.

alter the templating-abilities of **CPC** micelles. Furthermore, **SiO_2 ⊃ CPX** particles display a nonporous structure based on the adsorption isotherm, before and after calcination (Fig. S11), confirming that the described porosity is achieved only when **CPC** micelles are included in the silica nanoparticle.

Release studies were conducted to demonstrate the potential use of developed nanoparticles as drug delivery system. Nanoparticles were suspended in water and examined for antibiotic release overtime upon stirring. The presence of antibiotics was detected by absorption spectroscopy of the supernatant solutions following centrifugation to remove particles (Fig. 9). Dual loaded antimicrobial particles, **SiO_2 ⊃ CPC-CPX** (2 mg/mL) in water shows a time dependent cumulative release of **CPC** up to 12.9 ± 0.7 μg_{CPC}/mL after 48 h. In addition, **CPX** release 0.3 ± 0.1 μg_{CPX}/mL is observed after 48 h, illustrating release of both antimicrobials from **SiO_2 ⊃ CPC-CPX**. Instead, in **SiO_2 ⊃ CPX** (2 mg/mL), a maximum release at 48 h of 0.08 ± 0.03 μg_{CPX}/mL is observed (Fig. S12). Release from **SiO_2 ⊃ CPC-RIF** (2 mg/mL) in PBS buffer (pH 7.4), also shows a time dependent cumulative release of **CPC** up to 15.2 ± 0.6 μg_{CPC}/mL. The release of **RIF** is below the limit of detection for UV–Vis and therefore not quantified in this experiment, this is due to the low water solubility of **RIF** in addition to a low molar extinction coefficient. The presence of **RIF** in the supernatant is confirmed by mass spectrometry (Fig. S13). Finally, **SiO_2 ⊃ CPC** (2 mg/mL) particles in PBS buffer (pH 7.4) show a similar time dependent cumulative release up to 14.9 ± 1.0 μg_{CPC}/mL. Furthermore, methanol was chosen for the efficient disruption of the micelles as previously reported. [51] Release of the antibiotics from a suspension of nanoparticles was estimated: for **SiO_2 ⊃ CPC-CPX** (2 mg/mL) in methanol after 24 h as 6.4 ± 0.7 μg_{CPX}/mL and 140 ± 14 μg_{CPC}/mL. Similarly, for **SiO_2 ⊃ CPC-RIF**: in methanol 3.8 ± 1.5 μg_{RIF}/mL and 57 ± 5 μg_{CPC}/mL release was determined (Fig. S14). The quantity of antimicrobials released are within the Minimum Inhibitory Concentration values for susceptible bacteria strains, demonstrating the potential of the silica platform for their delivery. [52]

4. Conclusions

CPC micelles have shown to incorporate antibiotics in their structure which makes them promising vehicles for the loading of **CPX** and **RIF** antibiotics into silica nanoparticles. The antibiotic-**CPC** interactions were elucidated by ^{1}H NMR and NOESY experiments. The **CPC-CPX** interactions indicate that **CPX** is placed between the outer and palisade region of the **CPC** micelle. The NMR studies show that **RIF** is located further into the hydrophobic micelle core. The micelle incorporation of the antibiotics is also shown by a suite of analytical techniques. Introducing **CPC** micelles into SiO_2 nanoparticles led to a porous structure within the SiO_2 framework as shown by porosimetry studies, providing **CPC** as an ideal antimicrobial drug template, replacing toxic surfactants or polymers. The incorporated antibiotics can be released from silica particles due to disruption of the micelles alongside release of **CPC** molecules, providing a system of dual antimicrobial delivery. Our results represent a novel strategy for the development of porous SiO_2 using a therapeutic template which can find applications in enhancing loading and release of poorly-water soluble antibiotics.

CRediT authorship contribution statement

Asier R. Muguruza: Writing – original draft, Investigation, Formal analysis, Conceptualization. **Maria L. Odyniec:** Writing – original draft, Methodology, Formal analysis, Conceptualization. **Menisha Manhota:** Writing – review & editing, Methodology, Investigation, Formal analysis, Conceptualization. **Zaina Habib:** Investigation. **Knut Rurack:** Writing – review & editing. **Jessica M.A. Blair:** Supervision. **Sarah Kuehne:** Writing – review & editing, Supervision. **A. Damien Walmsley:** Writing – review & editing, Supervision. **Zoe Pikramenou:** Writing – review & editing, Writing – original draft, Supervision, Conceptualization.

Declaration of competing interest

The authors declare that they have no known competing financial

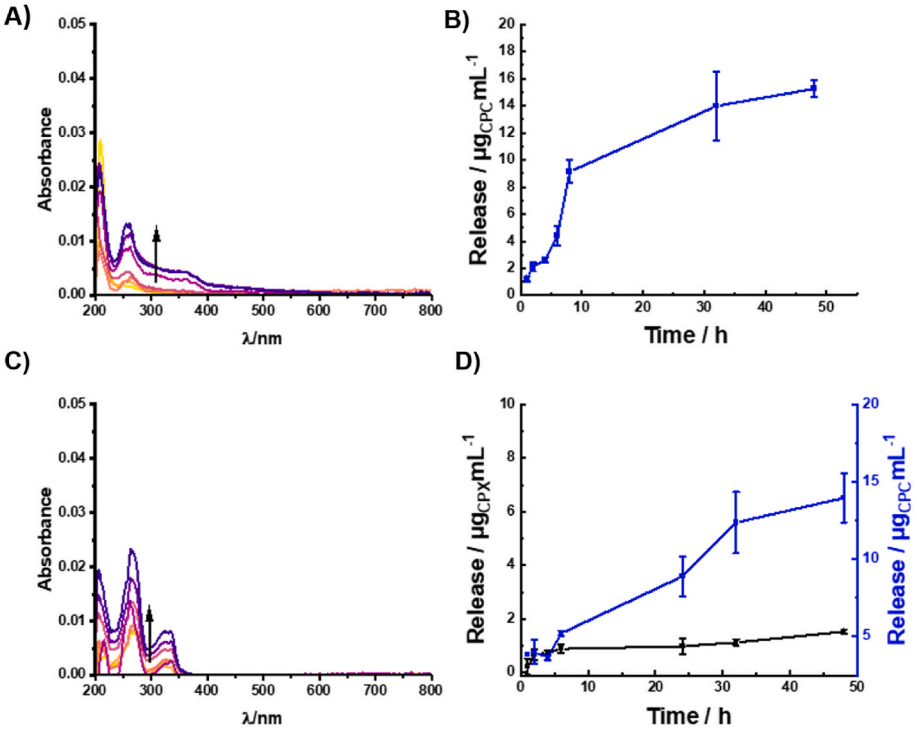

Fig. 9. (A, C) Representative absorption spectra of release studies of (A) **CPC** from **SiO_2⊃CPC-RIF** and (C) **CPX** and **CPC** from **SiO_2⊃CPC-CPX** in PBS buffer (pH 7.4) at 25 °C. (B, D) Cumulative release of (B) **CPC** from **SiO_2⊃CPC-RIF** and (D) **CPX** and **CPC** from **SiO_2⊃CPC-CPX** in PBS buffer (pH 7.4) at 25 °C.

interests or personal relationships that could have appeared to influence the work reported in this paper.

Data availability

Data will be made available on request.

Acknowledgements

The authors wish to acknowledge the funding agencies for support: Biotechnology and Biological Sciences Research Council (BBRSC) BB/M01116X/1 MIBTP (A.R.M.), and Engineering and Physical Sciences Research Council (EPSRC) EP/V028553/1, *SONATA* project (M.L.O., Z. P.) and EP/L016346/1 *Sci-Phy-4-Health* (M.M.). The authors would like to acknowledge Dr. Cécile Le Duff for her assistance with the NMR experiments.

Appendix A. Supplementary data

Supplementary data to this article can be found online at https://doi.org/10.1016/j.micromeso.2023.112841.

References

[1] A.B. Nik, H. Zare, S. Razavi, H. Mohammadi, P.T. Ahmadi, N. Yazdani, M. Bayandori, N. Rabiee, J.I. Mobarakeh, Smart drug delivery: capping strategies for mesoporous silica nanoparticles, Microporous Mesoporous Mater. 229 (2020), 110115, https://doi.org/10.1016/j.micromeso.2020.110115.

[2] J. Allouche, A. Le Beulze, J.C. Dupin, J.B. Ledeuil, S. Blanc, D. Gonbeau, Hybrid spiropyran-silica nanoparticles with a core-shell structure: sol-gel synthesis and photochromic properties, J. Mater. Chem. 20 (2010) 9370–9378, https://doi.org/10.1039/C0JM01780A.

[3] X. Li, D. Li, Z. Liu, Superiority of biomimetric micelle-entrapped nanoporous silica xerogel to deliver poorly water-soluble itraconazole, RSC Adv. 12 (2022) 28422–28432, https://doi.org/10.1039/D2RA04698A.

[4] J.M.V. Makabenta, A. Nabawy, C.H. Li, S. Schmidt-Malan, R. Patel, V.M. Rotello, Nanomaterial-based therapeutics for antibiotic-resistant bacterial infections, Nat. Rev. Microbiol. 19 (2021) 23–36, https://doi.org/10.1038/s41579-020-0420-1.

[5] M. Vallet-Regí, F. Schüth, D. Lozano, M. Colilla, M. Manzano, Engineering mesoporous silica nanoparticles for drug delivery: where are we after two decades? Chem. Soc. Rev. 51 (2022) 5365–5451, https://doi.org/10.1039/D1CS00659B.

[6] T. Asefa, Z. Tao, *Chem.*., Biocompatibility of mesoporous silica nanoparticles, Res. Toxicol. 25 (2012) 2265–2284, https://doi.org/10.1021/tx300166u.

[7] G.C. Carvalho, G.D. Marena, J.C.F. Karnopp, J. Jorge, R.M. Sábio, M.A.U. Martines, T.M. Bauab, M. Chorilli, Cetyltrimethylammonium bromide in the synthesis of mesoporous silica nanoparticles: general aspects and in vitro toxicity, Adv. Colloid Interface Sci. 307 (2022), 102746, https://doi.org/10.1016/j.cis.2022.102746.

[8] E. Ito, K.W. Yip, D. Katz, S.B. Fonseca, D.W. Hedley, S. Chow, G.W. Xu, T.E. Wood, C. Bastianutto, A.D. Schimmer, S.O. Kelley, F.F. Liu, Potential use of cetrimonium bromide as an apoptosis-promoting anticancer agent for head and neck cancer, Mol. Pharmacol. 76 (2009) 969–983, https://doi.org/10.1124/mol.109.055277.

[9] Z. Lui, D. Lui, L. Wang, J. Zhang, N. Zhang, Docetaxel-loaded Pluronic P123 polymeric micelles: *in vitro* and *in vivo* evaluation, Int. J. Mol. Sci. 12 (3) (2011) 1684–1696, https://doi.org/10.3390/ijms12031684.

[10] N.K. Mal, M. Fujiwara, Y. Tanaka, Photocontrolled reversible release of guest molecules from coumarin-modified mesoporous silica, Nature 421 (2003) 350–353, https://doi.org/10.1038/nature01362.

[11] C.-A. Cheng, T. Deng, F.-C. Lin, Y. Cai, J.I. Zink, Supramolecular nanomachines as stimuli-responsive gatekeepers on mesoporous silica nanoparticles for antibiotic and cancer drug delivery, Theranostics 9 (2019) 3341–3364, https://doi.org/10.7150/thno.34576.

[12] C.A. Stewart, Y. Finer, B.D. Hatton, Drug self-assembly for synthesis of highly-loaded antimicrobial drug-silica particles, Sci. Rep. 8 (2018) 895–906, https://doi.org/10.1038/s41598-018-19166-8.

[13] A. Brezhnev, F.-K. Tang, C.-S. Kwan, M.S. Basabrain, J.K.H. Tsoi, J.P. Matinlinna, P. Neelakantan, K.C.-F. Leung, One-pot preparation of cetylpyridinium chloride-containing nanoparticles for biofilm eradication, ACS Appl. Bio Mater. 6 (2023) 1221–1230, https://doi.org/10.1021/acsabm.2c01080.

[14] D. Khushalani, A. Kuperman, N. Coombs, G.A. Ozin, Mixed surfactant assemblies in the synthesis of mesoporous silicas, Chem. Mater. 8 (8) (1996) 2188–2193, https://doi.org/10.1021/cm9600945.

[15] V. Dubovoy, A. Ganti, T. Zhang, H. Al-Tameemi, J.D. Cerezo, J.M. Boyd, T. Asefa, One-pot hydrothermal synthesis of benzalkonium-templated mesostructured silica antibacterial agents, J. Am. Chem. Soc. 140 (2018) 13534–13537, https://doi.org/10.1021/jacs.8b04843.

[16] D.J. Lewis, V. Dore, M.J. Goodwin, A.C. Savage, G.B. Nash, P. Angeli, Z. Pikramenou, Luminescent ruthenium(II) tris-bipyridyl complex caged in nanoscale silica for particle velocimetry studies in microchannels, Meas. Sci. Technol. 23 (2012), 084004, https://doi.org/10.1088/0957-0233/23/8/084004.

[17] A.N. Dosumu, S. Claire, L.S. Watson, P.M. Girio, S.A.M. Osborne, Z. Pikramenou, N. J. Hodges, Quantification by luminescence tracking of red emissive gold nanoparticles in cells, JACS Au 1 (2021) 174–186, https://doi.org/10.1021/jacsau.0c00033.

[18] D.J. Lewis, V. Dore, N.J. Rogers, T.K. Mole, G.B. Nash, P. Angeli, Z. Pikramenou, Silica nanoparticles for micro-particle imaging velocimetry: fluorosurfactant improves nanoparticle stability and brightness of immobilised iridium(iii) complexes, Langmuir 29 (2013) 14701–14708, https://doi.org/10.1021/la403172m.

[19] A.R. Muguruza, A. di Maio, N.J. Hodges, J.M.A. Blair, Z. Pikramenou, Chelating silica nanoparticles for efficient antibiotic delivery and particle imaging in Gram-negative bacteria, Nanoscale Adv. 5 (2023) 2453, https://doi.org/10.1039/D2NA00884J.

[20] X. Mao, D.L. Aue, W. Buchalla, K.A. Hiller, T. Maisch, E. Hellwig, A. Al-Ahmad, F. Cieplik, Cetylpyridinium chloride: mechanism of action, antimicrobial efficacy in biofilms, and potential risk of resistance, Antimicrob. Agents Chemother. 64 (2020), e00576, https://doi.org/10.1128/AAC.00576-20, 20.

[21] S. Wu, Y. Huang, J. Yan, Y. Li, J. Wang, Y.Y. Yang, P. Yauan, X. Ding, Bacterial outer membrane-coated mesoporous silica nanoparticles for targeted delivery of antibiotic rifampicin against gram-negative bacterial infection in vivo, Adv. Funct. Mater. 31 (2021), 2103442, https://doi.org/10.1002/adfm.202103442.

[22] Q. Liu, Y. Zhang, J. Huang, Z. Xu, X. Li, J. Yang, H. Huang, S. Tang, Y. Chai, J. Lin, C. Yang, J. Liu, S. Lin, Mesoporous silica-coated silver nanoparticles as ciprofloxacin/siRNA carriers for accelerated infected wound healing, J. Nanotechnol. 20 (2022) 386, https://doi.org/10.1186/s12951-022-01600-9.

[23] B. de Juan Mora, L. Filipe, A. Forte, M.M. Santos, C. Alves, F. Teodoro, R. Pedrosa, M.R. Carrott, L.C. Branco, S. Gago, Boosting antimicrobial activity of ciprofloxacin by functionalization of mesoporous silica nanoparticles, Pharmaceuticals 13 (2021) 218, https://doi.org/10.3390/pharmaceutics13020218.

[24] D. Zhang, Z. Wu, J. Xu, J. Liang, J. Li, W. Yang, Tuning the emission properties of $Ru(phen)_3^{2+}$ doped silica nanoparticles by changing the addition time of the dye during the stöber process, Langmuir 26 (2010) 6657–6662, https://doi.org/10.1021/la903995r.

[25] I. Molinero, M.L. Sierra, M. Valiente, E. Rodenas, Physical properties of cetylpyridinium chloride micelles and their behaviours as reaction media, J. Chem. Soc., Faraday Trans. 92 (1996) 59–63, https://doi.org/10.1039/FT9969200059.

[26] D. Varade, T. Joshi, V.K. Aswal, P.S. Goyal, P.A. Hassan, P. Bahadur, Effect of salt on the micelles of cetyl pyridinium chloride, Colloids Surfaces A Physicochem. Eng. Asp. 259 (2005) 95–101, https://doi.org/10.1016/j.colsurfa.2005.02.018.

[27] R. Verma, A. Mishra, K.R. Mitchell-Koch, Molecular modelling of cetylpyridinium bromide, a cationic surfactant, in solution and micelle, J. Chem. Theor. Comput. 11 (2015) 5415–5425, https://doi.org/10.1021/acs.jctc.5b00475.

[28] J. Mirtič, A. Paudel, P. Laggner, S. Hudoklin, M.E. Kreft, J. Kristl, Polyelectrolyte-surfactant-complex nanoparticles as a delivery platform for poorly soluble drugs: a case study of ibuprofen loaded cetylpyridinium-alginate system, Int. J. Pharm. 580 (2020), 119199, https://doi.org/10.1016/j.ijpharm.2020.119199.

[29] A. Srivastava, K. Ismail, Binding of phenol red to cetylpyridinium chloride at air-solution and micelle-solution interfaces in aqueous ethylene glycol media, Colloids Surfaces A Physicochem. Eng. Asp. 462 (2014) 115–123, https://doi.org/10.1016/j.colsurfa.2014.08.021.

[30] T. Mondol, P. Rajdev, A. Makhal, S.K. Pal, Interaction of an antituberculosis drug with a nanoscopic macromolecular assembly: temperature-dependent förster resonance energy transfer studies on rifampicin in an anionic sodium dodecyl sulfate micelle, J. Phys. Chem. B 115 (2011) 2924–2930, https://doi.org/10.1021/jp108115h.

[31] A. Barve, A. Jain, H. Liu, Z. Zhao, K. Cheng, Enzyme-responsive polymeric micelles of cavazitaxel for prostate cancer targeted therapy, Acta Biomater. 113 (2020) 501–511, https://doi.org/10.1016/j.actbio.2020.06.019.

[32] Y. Wang, X. Ke, Z.X. Voo, S.S.L. Yap, C. Yang, S. Gao, S. Liu, S. Venkataraman, S.A. O. Obuobi, J.S. Khara, Y.Y. Yang, P.L.R. Ee, Biodegradable functional polycarbonate micelles for controlled release of amphotericin B, Acta Biomater. 46 (2016) 211–220, https://doi.org/10.1016/j.actbio.2016.09.036.

[33] S.D. Choudhury, N. Barooah, V.K. Aswal, H. Pal, A.C. Bhasikuttan, J. Mohanty, Stimuli-responsive supramolecular micellar assemblies of cetylpyridinium chloride with curcubit[5/7]urils, Soft Matter 10 (2014) 3485–3493, https://doi.org/10.1039/C3SM52024B.

[34] K. Xu, H.-Q. Ren, G.-M. Zeng, L.-L. Ding, J.-H. Huang, Investigation of interaction between phenol and cetylpyridinium micelle in absence and presence of electrolyte by ^{1}H NMR spectroscopy, Colloids Surfaces A Physicochem. Eng. Asp. 356 (2010) 150–155, https://doi.org/10.1016/j.colsurfa.2010.01.011.

[35] J.P. Mata, V.K. Aswal, P.A. Hassan, P. Bahadur, A phenol-induced structural transition in aqueous cetyltrimethylammonium bromide solution, J. Colloid Interface Sci. 299 (2006) 910–915, https://doi.org/10.1016/j.jcis.2006.02.032.

[36] U. Tehler, J.H. Fagerberg, R. Svensson, M. Larhed, P. Artursson, C.A.S. Bergström, Optimising solubility and permeability of a biopharmaceutics classification system (bcs) class 4 antibiotic drug using lipophilic fragments disturbing the crystal lattice, J. Med. Chem. 56 (2013) 2690–2694, https://doi.org/10.1021/jm301721e.

[37] A. Czyrski, J. Sznura, The application of Box-Behnken-Design in the optimization of HPLC separation of fluoroquinolones, Sci. Rep. 9 (2019) 1–10, https://doi.org/10.1038/s41598-019-55761-z.

[38] D.L. Ross, C.M. Riley, Aqueous stability of some variously substituted quinolone antimicrobials, Int. J. Pharm. 63 (1990) 237–250. https://doi.org/10.1016/0378-5173(90)90130-V.

[39] B.J. Kim, S.S. Im, S.G. Oh, Investigation on the solubilization locus of aniline-HCl salt in SDS micelles with ^{1}H NMR spectroscopy, Langmuir 17 (2001) 565–566, https://doi.org/10.1021/la0012889.

[40] N. Maurer, K.F. Wong, M.J. Hope, P.R. Cullis, Anomalous solubility behaviour of the antibiotic ciprofloxacin encapsulated in liposomes: a ^{1}H-NMR study, Biochim. Biophys. Acta - Biomembr. 1374 (1998) 9–20, https://doi.org/10.1016/s0005-2736(98)00125-4.

[41] C.M. Franzin, X.M. Gong, K. Thai, J. Yu, F.M. Marassi, NMR of membrane proteins in micelles and bilayers: the FXYD family proteins, Methods 41 (2007) 398–408, https://doi.org/10.1016/j.ymeth.2006.08.011.

[42] W. Chen, S.A. Elfeky, Y. Nonne, L. Male, K. Ahmed, C. Amiable, P. Axe, S. Yamada, T.D. James, S.D. Bull, J.S. Fossey, A pyridinium cation-π interaction sensor for the fluorescent detection of alkyl halides, Chem. Commun. 47 (2011) 253–255, https://doi.org/10.1039/C0CC01420F.

[43] Y.J. Huang, Y.B. Jiang, S.D. Bull, J.S. Fossey, T.D. James, Diols and anions can control the formation of an exciplex between pyridinium boronic acid with an aryl group connected *via* a propylene linker, Chem. Commun. 46 (2010) 8180–8182, https://doi.org/10.1039/C0CC03099F.

[44] E.V. Pletneva, A.T. Laederach, D.B. Fulton, N.M. Kostić, The role of cation-π interactions in biomolecular association. the design of peptides favouring interactions between cationic and aromatic amino acid side chains, J. Am. Chem. Soc. 123 (2001) 6232–6245, https://doi.org/10.1021/ja010401u.

[45] Q. Zhao, S. Zhang, X. Zhang, L. Lei, W. Ma, C. Ma, L. Song, J. Chen, B. Pan, B. Xing, Cation-Pi Interaction: a key force for sorption of fluoroquinolone antibiotics on pyrogenic carbonaceous materials, Environ. Sci. Technol. 51 (2017) 13659–13667, https://doi.org/10.1021/acs.est.7b02317.

[46] H.Ç. Arca, L.I. Mosquera-Giraldo, J.M. Pereira, N. Sriranganathan, L.S. Taylor, K. J. Edgar, Rifampicin stability and solution concentration enhancement through amorphous solid dispersion in cellulose ω-carboxyalkanoate matrices, J. Pharmaceut. Sci. 107 (2018) 127–138, https://doi.org/10.1016/j.xphs.2017.05.036.

[47] M. Motiei, L. Pleno de Gouveia, T. Šopík, R. Vícha, D. Škoda, J. Císař, R. Khalili, E. Domincová Bergerová, L. Münster, H. Fei, V. Sedlařík, P. Sáha, Nanoparticle-based rifampicin delivery system development, Molecules 26 (2021) 1–19, https://doi.org/10.3390/molecules26072067.

[48] G. De Guidi, G. Bracchitta, A. Catalfo, Photosensitization reactions of fluoroquinolones and their biological consequences, Photochem. Photobiol. 87 (2011) 1214–1229, https://doi.org/10.1111/j.1751-1097.2011.00978.x.

[49] A.R. Soemo, J.E. Pemberton, Combined quenching mechanism of anthracene fluorescence by cetylpyridinium chloride in sodium dodecyl sulfate micelles, J. Fluoresc. 24 (2014) 295–299, https://doi.org/10.1007/s10895-013-1319-2.

[50] J.W.M. Osterrieth, J. Rampersad, D. Madden, N. Rampal, L. Skoric, B. Connolly, M. D. Allendorf, V. Stavila, J.L. Snider, R. Ameloot, J. Marreiros, C. Ania, D. Azevedo, E. Vilarrasa-Garcia, B.F. Santos, X.H. Bu, Z. Chang, H. Bunzen, N.R. Champness, S. L. Griffin, B. Chen, R.B. Lin, B. Coasne, S. Cohen, J.C. Moreton, Y.J. Colón, L. Chen, R. Clowes, F.X. Coudert, Y. Cui, B. Hou, D.M. D'Alessandro, P.W. Doheny, M. Dincă, C. Sun, C. Doonan, M.T. Huxley, J.D. Evans, P. Falcaro, R. Ricco, O. Farha, K.B. Idrees, T. Islamoglu, P. Feng, H. Yang, R.S. Forgan, D. Bara, S. Furukawa, E. Sanchez, J. Gascon, S. Telalović, S.K. Ghosh, S. Mukherjee, M. R. Hill, M.M. Sadiq, P. Horcajada, P. Salcedo-Abraira, K. Kaneko, R. Kukobat, J. Kenvin, S. Keskin, S. Kitagawa, K. ichi Otake, R.P. Lively, S.J.A. DeWitt, P. Llewellyn, B.V. Lotsch, S.T. Emmerling, A.M. Pütz, C. Martí-Gastaldo, N. M. Padial, J. García-Martínez, N. Linares, D. Maspoch, J.A. Suárez del Pino, P. Moghadam, R. Oktavian, R.E. Morris, P.S. Wheatley, J. Navarro, C. Petit, D. Danaci, M.J. Rosseinsky, A.P. Katsoulidis, M. Schröder, X. Han, S. Yang, C. Serre, G. Mouchaham, D.S. Sholl, R. Thyagarajan, D. Siderius, R.Q. Snurr, R. B. Goncalves, S. Telfer, S.J. Lee, V.P. Ting, J.L. Rowlandson, T. Uemura, T. Iiyuka, M.A. van der Veen, D. Rega, V. Van Speybroeck, S.M.J. Rogge, A. Lamaire, K. S. Walton, L.W. Bingel, S. Wuttke, J. Andreo, O. Yaghi, B. Zhang, C.T. Yavuz, T. S. Nguyen, F. Zamora, C. Montoro, H. Zhou, A. Kirchon, D. Fairen-Jimenez, How reproducible are surface areas calculated from the bet equation? Adv. Mater. 34 (2022), 2201502 https://doi.org/10.1002/adma.202201502.

[51] R. Pazo-Llorente, C. Bravo-Díaz, E. González-Romero, Monitoring micelle breakdown by chemical trapping, Langmuir 19 (2003) 9142–9146, https://doi.org/10.1021/la034879i.

[52] J.M. Andrews, Determination of minimum inhibitory concentrations, J. Antimicrob. Chemother. 48 (2001) 5–16, https://doi.org/10.1093/jac/48.suppl_1.5.